THE JOURNAL OF BIOLOGICAL CHEMISTRY Vol. 277, No. 30, Issue of July 26, pp. 27240–27246, 2002
Printed in U.S.A.

Kinetics and Energetics of Assembly, Nucleation, and Growth of Aggregates and Fibrils for an Amyloidogenic Protein

INSIGHTS INTO TRANSITION STATES FROM PRESSURE, TEMPERATURE, AND CO-SOLUTE STUDIES*

Received for publication, March 14, 2002, and in revised form, April 23, 2002
Published, JBC Papers in Press, May 21, 2002, DOI 10.1074/jbc.M202492200

Yong-Sung Kim‡, Theodore W. Randolph§, Fred J. Stevens¶, and John F. Carpenter‡‖

From the ‡Department of Pharmaceutical Sciences, School of Pharmacy, University of Colorado Health Sciences Center, Denver, Colorado 80262, the §Department of Chemical Engineering, University of Colorado, Boulder, Colorado 80309, and the ¶Biosciences Division, Argonne National Laboratory, Argonne, Illinois 60439

The transition states for prenucleation assembly, nucleation, and growth of aggregates and amyloid fibrils were investigated for a dimeric immunoglobulin light chain variable domain, employing pressure, temperature, and solutes as variables. Pressure-induced aggregation was nucleation-dependent and first-order in protein concentration and could be seeded. The insoluble aggregates were mixtures of amyloid fibrils and amorphous aggregates. Activation volumes, activation surface areas, and activation waters of hydration were larger for aggregate growth than for prenucleation assembly or nucleation, although activation free energies were similar for the three processes. Activation free energies for each of the transition states were dominated by the unfavorable free energy of solvation of newly exposed surfaces. Equilibrium dissociation and unfolding of the dimer showed a much larger volume change than those required to form the transition states for the three processes. Thus, the transition states for these steps are similar to the native state, and their formation requires only small structural perturbations. Finally, the presence of Congo red during amyloid fibril formation shortened lag times and caused pressure insensitivity of nucleation, suggesting that this compound or its analogs may not be effective as inhibitors of amyloidosis.

Alzheimer's, Parkinson's, and Huntington's diseases and systemic amyloidosis are pathologies wherein proteins aggregate *in vivo* to form insoluble deposits (1, 2). *In vitro* studies have documented that many amyloidogenic proteins assemble irreversibly into fibrils via a nucleation-dependent pathway (3, 4). Protein aggregation occurs through specific intermediates, which are structurally perturbed relative to the native conformation (1, 5, 6). Numerous studies have focused on spectroscopic characterization of the aggregation-competent conformation under non-native conditions where it is highly populated. However, insight into the mechanisms of aggregation requires quantitative assessment of the transition state between the native protein and the aggregation-competent, structurally perturbed intermediate. Furthermore, strategies to inhibit aggregate formation should focus on increasing the energetic barriers to transition state formation.

In this study, we chose the immunoglobulin light chain (LC)[1] as a model amyloidogenic protein. LCs deposit pathologically *in vivo* as amyloid fibrils (light chain-associated amyloidosis) and amorphous granular aggregates (light chain deposition diseases) (2). We employed hydrostatic pressure, a co-solute (sucrose), and temperature to quantify the magnitude of the structural change (activation volume and specific surface area of activation) and energetics needed to form the transition states for prenucleation assembly, nucleation, and growth of LC aggregates and amyloid fibrils. Pressure is a fundamental variable that has often been manipulated to probe the thermodynamics and kinetics of protein folding and unfolding (7–10). However, the power of high-pressure studies to gain insight into transition states associated with protein aggregation has not been fully exploited; only a single study has been published, which characterized the transition state between the native and aggregation-competent forms of interferon-γ (11). Likewise, manipulation of solution thermodynamics by the addition of co-solutes such as sucrose can be used to characterize transition states associated with protein aggregation (11, 12), but this method has not been applied to an amyloidogenic protein. We used *in situ* high-pressure UV-visible spectroscopy to investigate the kinetics of aggregation and amyloid fibril nucleation and growth as well as the thermodynamics of unfolding and dissociation. Furthermore, we followed fibril formation under pressure using *in situ* Congo red (CR) binding.

EXPERIMENTAL PROCEDURES

Materials—Recombinant LC variable domain (V_L) SMA was expressed in *Escherichia coli* and purified (>99% by SDS-PAGE) as described previously (13). Recombinant SMA has the same sequence as the V_L that originated from lymph node-derived amyloid fibrils of a patient with light chain-associated amyloidosis (14). SMA forms both amorphous aggregates and amyloid fibrils, depending on solution conditions (15).

Dithiothreitol (DTT) and CR were purchased from Sigma. Highly purified sucrose was from Pfanstiehl Laboratories, Inc. Other chemicals were from Sigma and were of reagent or higher grade. All experiments were carried out in 10 mM Tris-HCl and 100 mM NaCl (pH 7.4) (buffer A), which is insensitive to pH change with pressure (9).

Pressure- and Urea-induced Equilibrium Unfolding—UV-visible absorbance spectra were measured using a high-pressure cell with two sapphire windows in a PerkinElmer Life Sciences Lambda 35 UV-visible spectrophotometer (11). Temperature was controlled within ±0.5 °C with a circulating ethylene glycol bath (Julabo F25) connected to a heat exchanger mounted on the bottom of the cell and was moni-

* The costs of publication of this article were defrayed in part by the payment of page charges. This article must therefore be hereby marked "*advertisement*" in accordance with 18 U.S.C. Section 1734 solely to indicate this fact.

‖ To whom correspondence should be addressed: Dept. of Pharmaceutical Sciences, School of Pharmacy, University of Colorado Health Sciences Center, 4200 E. 9th Ave., Denver, CO 80262. Tel.: 303-315-6075; Fax: 303-315-6281; E-mail: John.Carpenter@uchsc.edu.

[1] The abbreviations used are: LC, immunoglobulin light chain; CR, Congo red; V_L, light chain variable domain; DTT, dithiothreitol; MPa, megapascal(s); HPLC, high-performance liquid chromatography; ThT, thioflavin T; FT-IR, Fourier transform infrared; TEM, transmission electron microscopy.

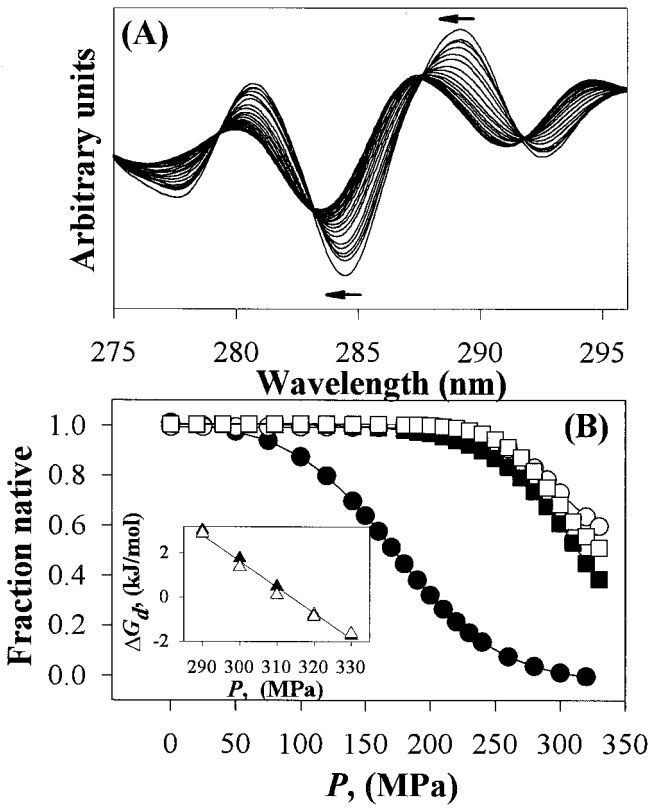

FIG. 1. **Pressure-induced dissociation and unfolding of SMA.** *A*, second-derivative UV spectra of 0.5 mg/ml SMA in 2 M urea at 32 °C as a function of pressure. *Arrows* indicate the spectral shifts with increasing pressure. *B*, f_N monitored as a function of pressure for 0.5 mg/ml SMA in 2 M urea (●) and in buffer A (○) at 32 °C and for 0.5 (■) and (□) 1 mg/ml SMA in buffer A at 37 °C. *Inset*, ΔG_d *versus* P for dissociation of 0.5 (▲) and (△) 1 mg/ml SMA in buffer A at 37 °C.

tored with a thermocouple inserted into the top of the pressure cell. 0.5 mg/ml SMA in buffer A with 2 M urea and 0.5 or 1 mg/ml SMA in buffer A were equilibrated overnight at room temperature, loaded into a 12-mm diameter × 13-mm height quartz cell, and placed in the high-pressure unit. After thermal equilibration, hydrostatic pressure was gradually increased to 330 MPa in 10- or 20-MPa increments. At each pressure, conformational transitions were monitored by recording second-derivative UV spectra from 270 to 300 nm at 0.1-nm intervals. Approximately 10 min were required to reach conformational equilibrium at each pressure. Urea-induced unfolding was also performed at atmospheric pressure for 0.5 mg/ml SMA at 32 °C after equilibration of the samples at room temperature overnight. Unfolding curves were constructed by plotting the wavelength of the intensity minimum around 284 nm of the second-derivative UV spectra, which reflects the polarity near tyrosine residues (16), *versus* pressure or [urea].

Aggregation Studies—All aggregation experiments were conducted in buffer A containing 10 mM DTT. Preliminary experiments indicated that the presence of DTT, which presumably reduces the intramolecular disulfide bridge between Cys-23 and Cys-88 in SMA (17), was required to foster protein aggregation under pressure at reasonable rates (*e.g.* process complete within 8 h; data not shown).

In pressure studies, 1 mg/ml SMA was incubated at 80, 120, 160, 200, and 240 MPa and 32 °C. Aggregation of 1 mg/ml SMA samples (200 MPa) was also measured at 30, 32, 34, 36, and 38 °C and at 32 °C in 0.125, 0.25, 0.5, 0.75, and 1 M sucrose. Aggregation rates as a function of protein concentration (200 MPa and 32 °C) were determined with 0.25, 0.5, 0.75, 1, and 1.25 mg/ml SMA. Aggregation was monitored by optical density at 320 nm (OD_{320}) as described for nucleation-dependent growth of Aβ peptides (3). Protein conformational transitions were monitored with second-derivative UV spectra. The time from application of pressure to acquisition of the first UV scan was ~10 min.

Effects of Seeding on Aggregation—To prepare "seeds," aggregates formed at 200 MPa and 32 °C were washed (three times) by centrifugation and resuspension with 1 volume of buffer A. The suspension was sonicated for 10 s and cooled on ice for 30 s (12 times) with output cycle 5 and 50% duty on a Branson sonifier (VWR Scientific). To prepare seeds from amyloid fibrils generated at atmospheric pressure, 1 mg/ml SMA in buffer A was agitated at 37 °C for 96 h (13) and sonicated as described above. To study effects of seeding on aggregation, samples containing 1 mg/ml SMA and 0.1 mg/ml seeds were incubated either at 200 MPa and 32 °C with 10 mM DTT or at atmospheric pressure and 37 °C with agitation in buffer A alone (13).

In Situ CR Binding Kinetics—A 300–400 μM CR stock solution was freshly prepared in water containing 10% (v/v) ethanol as described by Klunk *et al.* (18). Buffer A containing 1 mg/ml SMA with 10 mM DTT and 12 μM CR was incubated at 80, 120, 160, 200, and 240 MPa and 32 °C. As a non-aggregating control, a sample without DTT was incubated at 200 MPa and 32 °C. Spectra were collected between 350 and 700 nm every 3.2 min (18). To subtract the contributions from light scattering to the raw spectrum, a series of spectra from aggregation experiments without CR were obtained, and a reference spectrum was created by interpolation to match the OD_{700} of the raw spectrum in the presence of CR. The interpolated spectrum was subtracted from the raw spectrum using GRAMS/32® software (Galactic Industries Corp.). The resulting difference spectrum was used to calculate a second-derivative spectrum using a 120-point Savitsky-Golay derivative function with GRAMS/32® software. CR binding was monitored by the intensity of second-derivative spectra at 542 nm.

Size-exclusion High-performance Liquid Chromatography (HPLC), Thioflavin T (ThT) Assay, and Fourier Transform Infrared (FT-IR) Spectroscopy—At the completion of pressure-induced aggregation, pressure was released, and the aggregates were analyzed. To determine whether they were covalently cross-linked by disulfide bonds, aggregates were washed three times with buffer A by centrifugation and resuspension to remove DTT and analyzed by reducing and nonreducing SDS-PAGE. Aggregate pellets were also resuspended in 7 M guanidine HCl in buffer A, incubated for 1 h, and analyzed by size-exclusion HPLC. ThT assay for protein fibrils was performed as described (13, 19). FT-IR spectroscopy was used to determine the secondary structure of native SMA (20 mg/ml in buffer A), pure SMA amyloid fibrils (generated by incubation at atmospheric pressure by agitation for 96 h and concentrated 20-fold), and the insoluble aggregates formed under high pressure after washing three times with buffer A and concentrating 20-fold (13, 19).

Transmission Electron Microscopy (TEM) and CR Staining of Precipitated Protein—CR binding to precipitates was assessed as previously described (19, 20). TEM was performed as described (13) after DTT was removed from the aggregates by centrifugation and resuspension with 1 volume of buffer A.

Thermodynamic and Kinetic Data Analyses—The linear extrapolation method was used to calculate the fraction of native protein (f_N) present during pressure- and urea-induced unfolding (19, 21). From data for urea-induced dissociation and unfolding at atmospheric pressure, the free energy of dissociation in buffer A alone, ΔG_d (buffer A), was obtained by extrapolation of the plot of ΔG_d *versus* [urea] to 0 M urea, where $\Delta G_d = -RT\ln(4C_0(1 - f_N)^2/f_N)$, and C_0 is the initial protein concentration in mg/ml, R is the gas constant, and T is temperature (7, 10). The choice of mg/ml units for C_0 implies a reference state of 1 mg/ml SMA. For the pressure experiments in the absence of urea, unfolding was incomplete due to experimental pressure limitations of the UV cell. f_N was estimated using the post-transition region base line from the pressure-induced unfolding curve in the presence of 2 M urea in which complete unfolding occurred (11, 21).

The equilibrium dissociation volume change (ΔV_d) for the homodimer of SMA was obtained in the transition region of unfolding from the slope of a plot of ΔG_d *versus* P, where P is the pressure (7, 10). The free energy of dissociation at atmospheric pressure, ΔG_d (0.1 MPa), was extrapolated from pressure-induced unfolding data (Equation 1) (11),

$$\Delta G_d(0.1\ \text{MPa}) = \Delta G_d(P_{1/2}) - P_{1/2}\Delta V_d \qquad \text{(Eq. 1)}$$

where $P_{½}$ is the pressure at which f_N is 0.5 (10, 11).

For the aggregation studies, the lag time, t_{lag} (min), for nucleation was calculated by extrapolation of the linear region of the growth phase to the base line of the lag phase (13). The nucleation rate constant was determined by $1/t_{lag}$ (min^{-1}). The first-order prenucleation assembly rate constant, k_{prenuc} (min^{-1}), and the growth rate constant, k_{growth} (min^{-1}), were determined from the initial maximum slope of the plot of $\ln((OD_{320,f} - OD_{320,t})/(OD_{320,f} - OD_{320,0}))$ *versus* time in the prenucleation assembly and growth regions, respectively, where $OD_{320,f}$ is the final OD_{320} and $OD_{320,t}$ is at time = t and $OD_{320,0}$ is at time = 0. For the CR binding kinetics, the intensity of second-derivative absorbance spectra at 542 nm was used instead of OD_{320}. From the pressure-dependent aggregation kinetics, the partial molar volume changes (ΔV^*) between the native state (N) and the aggregation transition state (N^*) were

TABLE I
Thermodynamic parameters for pressure-induced dissociation and unfolding of SMA

The reference state is 1 mg/ml SMA, and ± values indicate 95% confidence limits from linear regression.

SMA conc	ΔV_d	$P_{1/2}$	ΔG_d (0.1 MPa)
	ml/mol	*MPa*	*kJ/mol*
0.5 mg/ml in 2 M urea at 32 °C	−99 ± 4	172 ± 1	17 ± 1
0.5 mg/ml at 32 °C	−105 ± 22	342 ± 5	36 ± 8
0.5 mg/ml at 37 °C	−121 ± 12	315 ± 2	38 ± 4
1 mg/ml at 37 °C	−113 ± 28	329 ± 6	39 ± 10

determined for prenucleation assembly (ΔV^*_{prenuc}), nucleation (ΔV^*_{nuc}), and growth (ΔV^*_{growth}) using Equations 2–4 (8).

$$\left(\frac{\partial RT\ln k_{prenuc}}{\partial P}\right)_T = -\Delta V^*_{prenuc} \quad \text{(Eq. 2)}$$

$$\left(\frac{\partial RT\ln(1/t_{lag})}{\partial P}\right)_T = -\Delta V^*_{nuc} \quad \text{(Eq. 3)}$$

$$\left(\frac{\partial RT\ln k_{growth}}{\partial P}\right)_T = -\Delta V^*_{growth} \quad \text{(Eq. 4)}$$

The specific molar surface area changes (Δa^*) between N and N^* were determined from sucrose concentration-dependent aggregation kinetics for prenucleation assembly (Δa^*_{prenuc}), nucleation (Δa^*_{nuc}), and growth (Δa^*_{growth}), respectively, by Equations 5–7 (12),

$$\left(\frac{\partial RT\ln k_{prenuc}}{\partial \sigma}\right)_{P,T} = -\Delta a^*_{prenuc} \quad \text{(Eq. 5)}$$

$$\left(\frac{\partial RT\ln(1/t_{lag})}{\partial \sigma}\right)_{P,T} = -\Delta a^*_{nuc} \quad \text{(Eq. 6)}$$

$$\left(\frac{\partial RT\ln k_{growth}}{\partial \sigma}\right)_{P,T} = -\Delta a^*_{growth} \quad \text{(Eq. 7)}$$

where σ is surface tension (22).

The apparent activation energies (E_a) for prenucleation assembly, nucleation, and growth were determined from Arrhenius plots (23). Activation enthalpies (ΔH^*) and activation entropies (ΔS^*) for each transition were calculated using the Eyring transition model (23) and used for the calculation of activation free energies (ΔG^*) using $\Delta G^* = \Delta H^* - T\Delta S^*$. ΔG^*, $T\Delta S^*$, and ΔH^* were separated into those from solvation (ΔG^*_{solv}, $T\Delta S^*_{solv}$, and ΔH^*_{solv}) and those arising from all other effects, including protein conformational changes (ΔG^*_{conf}, $T\Delta S^*_{conf}$, and ΔH^*_{conf}). ΔG^*_{solv} was estimated from a surface tension of water at 32 °C of 42.6 kJ/mol/nm^2 (24) multiplied by the measured Δa^* for each transition state. ΔS^*_{solv} was estimated from a reported value for entropy of hydration of −4.2 J/mol/K/water molecule (25) multiplied by the average value of changes in waters of hydration between N and N^* (Δn_w^*), which was determined from ΔV^* and Δa^* for each transition state (11). Errors associated with parameters obtained from linear regression are reported as 95% confidence limits on the fit.

RESULTS

Pressure-induced Equilibrium Unfolding—Fig. 1*A* shows the second-derivative UV spectra of SMA as a function of pressure up to 330 MPa in 2 M urea at 32 °C. At atmospheric pressure, the midpoint for urea-induced dissociation and unfolding of 0.5 mg/ml SMA was 4.4 M urea, and the onset for unfolding occurred at 2.8 M urea (data not shown). The pressure-induced equilibrium unfolding curve was typical of a two-state transition (Fig. 1*B*), with clear isosbestic points in second-derivative UV spectra (Fig. 1*A*). In the absence of urea, unfolding was incomplete over this pressure range. Unfolding curves (37 °C) shifted to higher pressures with increases in protein concentration (Fig. 1*B*). A plot of ΔG_d *versus* P for the two protein concentrations yielded a straight line ($r^2 = 0.99$) (Fig. 1*B*, *inset*), strongly suggesting that dissociation is concomitant with protein unfolding (7, 10, 11). Pressure-induced dissociation was >98% reversible for all experiments.

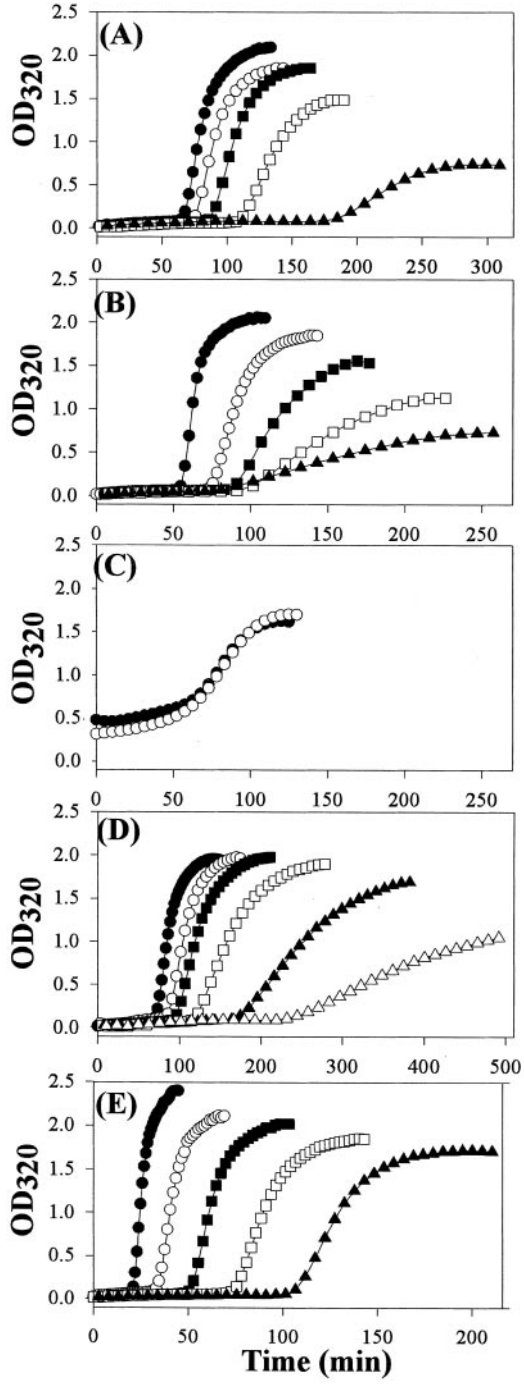

FIG. 2. **Pressure-induced SMA aggregation kinetics monitored at OD_{320}.** *A*, protein concentration-dependent aggregation at 200 MPa and 32 °C for 0.25 (▲), 0.5 (□), 0.75 (■), 1.0 (○), and 1.25 (●) mg/ml. *B*, pressure-dependent aggregation with 1 mg/ml SMA at 32 °C and 80 (▲), 120 (□), 160 (■), 200 (○), and 240 (●) MPa. *C*, seeding studies for 1 mg/ml SMA at 200 MPa and 32 °C with seeds from high pressure-induced aggregates (●) and pure SMA amyloid fibrils produced at atmospheric pressure (○). *D*, sucrose concentration-dependent aggregation with 1 mg/ml SMA at 200 MPa and 32 °C in 0 (●), 0.125 (○), 0.25 (■), 0.5 (□), 0.75 (▲), and 1.0 (△) M sucrose. *E*, temperature-dependent aggregation with 1 mg/ml SMA at 200 MPa and 30 °C (▲), 32 °C (□), 34 °C (■), 36 °C (○), and 38 °C (●).

From pressure-induced dissociation data, ΔV_d, $P_{½}$, and ΔG_d (0.1 MPa) were calculated (Table I). ΔV_d values were independent of protein concentration and temperature within experimental errors, with an average value of −113 ± 11 ml/mol. The partial molar surface area change for dissociation (Δa_d) was

estimated as 9.0 nm^2/molecule by $\Delta a_d = -0.079 \times \Delta V_d$ (11). ΔG_d (0.1 MPa) estimated from pressure-induced dissociation of 0.5 mg/ml SMA at 32 °C (36 ± 8 kJ/mol) was the same as that determined by urea-induced unfolding (38 ± 5 kJ/mol).

Aggregation Kinetics—In the absence of DTT, insoluble aggregates of SMA (1 mg/ml) did not form under pressure (*e.g.* 100 MPa at 37 °C for 3 days) even in the presence of urea (0–5 M) (data not shown). Thus, all the aggregation studies under high pressure were performed in buffer A containing 10 mM DTT.

Pressure-, protein concentration-, sucrose concentration-, and temperature-dependent aggregation under high pressure showed kinetics typical of nucleation-dependent growth (Fig. 2), characterized by an initial lag phase, followed by an exponential growth phase (3, 4). Prenucleation assembly rates increased, nucleation lag times decreased, and exponential growth rates increased with increases in protein concentration, pressure, and temperature and with decreases in sucrose concentration (Fig. 2). The aggregation kinetics were highly reproducible, *e.g.* $k_{\text{prenuc}} = 6 \times 10^{-4} \pm 4 \times 10^{-5}$ min^{-1}, $t_{\text{lag}} = 71.2 \pm 3.1$ min, and $k_{\text{growth}} = 0.060 \pm 0.001$ min^{-1} (mean ± S.D.) for triplicate samples of 1 mg/ml SMA at 200 MPa and 32 °C. At 200 MPa, prenucleation assembly, nucleation, and growth kinetics were first-order in protein concentration, as determined from the slopes of log-log plots of prenucleation assembly rates (0.92 ± 0.59, $r^2 = 0.92$), $1/t_{\text{lag}}$ (0.72 ± 0.08, $r^2 = 0.99$), and growth rates (1.29 ± 0.33, $r^2 = 0.98$), respectively, *versus* dimer concentration. Interestingly, in all instances, nucleation occurred only after OD_{320} reached 0.10 ± 0.02 (Fig. 2), implying that the critical nucleus size is independent of pressure, sucrose concentration, protein concentration, and temperature over the ranges studied.

Values for $\Delta V^*_{\text{prenuc}}$, ΔV^*_{nuc}, and $\Delta V^*_{\text{growth}}$ (Table II) corresponded to ~13, 11, and 26% of ΔV_d, respectively. Similarly, values for $\Delta a^*_{\text{prenuc}}$, Δa^*_{nuc}, and $\Delta a^*_{\text{growth}}$ (Table II) were ~17, 18, and 32% of Δa_d, respectively. As Webb *et al.* (11) described in detail, ΔV^* and Δa^* can be interconverted and can be used to estimate changes in waters of hydration (Δn_w^*) assuming that pressure effects are dominated by exposure of hydrophobic groups to water. Measured and interconverted ΔV^* and Δa^* values for prenucleation assembly, nucleation, and growth showed internal consistency (Table II). Δn_w^* values for prenucleation assembly, nucleation, and growth were estimated as 9, 8, and 18 mol of H_2O/mol of dimer from ΔV^* and 12, 12, and 23 mol of H_2O/mol of dimer from Δa^*, respectively.

Prenucleation assembly, nucleation, and growth showed Arrhenius temperature dependence (data not shown). ΔG^* was equivalent for each process (Table III). E_a and ΔH^* were equivalent for nucleation and growth, whereas E_a, ΔH^*, and $T\Delta S^*$ for prenucleation assembly were smaller than those for the other transitions (Table III). For each process, ΔG^* was dominated by solvation effects. $T\Delta S^*_{\text{solv}}$ values were negative for all three processes, whereas $T\Delta S^*_{\text{conf}}$ values were positive (Table III).

Aggregate Characterization—At the end of pressure-induced aggregation, pressure was released, and the final aggregates were analyzed by several methods. Reducing and nonreducing SDS-PAGE showed only SMA monomers (data not shown). Furthermore, when aggregates were placed in 7 M guanidine HCl in buffer A, they immediately redissolved, and only dimeric SMA was detected by size-exclusion HPLC (data not shown). Thus, the aggregates were not covalently cross-linked.

The secondary structures of the precipitated aggregates were compared with that of native SMA by FT-IR spectroscopy. The FT-IR spectrum of native SMA has a dominant band at 1638 cm^{-1}, indicating that the native protein is composed predominantly of β-sheet (Fig. 3), which is characteristic of the V_L (15, 19). FT-IR spectra of pressure-induced aggregates and pure SMA amyloid fibrils (generated by incubation at atmospheric pressure by agitation for 96 h) had dominant bands around 1625–1627 and 1689–1693 cm^{-1} (Fig. 3), which are characteristic of non-native intermolecular antiparallel β-sheet (15, 19, 26). Other aggregates formed at various protein concentrations, temperatures, and sucrose concentrations showed similar FT-IR spectra (data not shown), indicating that the main secondary structures of all aggregates are non-native intermolecular antiparallel β-sheet.

The ThT fluorescence intensity of the aggregates was proportional to the final OD_{320} noted under pressure, with ThT = $1.45 \times OD_{320,f}$ ($r^2 = 0.89$) (Table IV). Thus, the aggregates contained amyloid fibrils. But the ThT values were about one-tenth to one-fifth of that for pure SMA amyloid fibrils gener-

TABLE II
Kinetic parameters for the formation of N for prenucleation assembly, nucleation, and growth of SMA aggregation*

Boldface values were from experimental data, and other values were calculated as described in detail in Table II of Webb *et al.* (11). ± values indicate the 95% confidence limits from linear regression.

Parameters	*P* effects	σ effects
$\Delta V^*_{\text{prenuc}}$, ml/mol dimer	**−14.5 ± 3.0**	−18.9
$\Delta a^*_{\text{prenuc}}$, nm^2/molecule	1.2	**1.5 ± 0.3**
$\Delta n_w^*{}_{\text{prenuc}}$, mol H_2O/mol dimer	8.9	11.6
ΔV^*_{nuc}, ml/mol dimer	**−12.4 ± 6.7**	−20.2
Δa^*_{nuc}, nm^2/molecule	1.0	**1.6 ± 0.3**
$\Delta n_w^*{}_{\text{nuc}}$, mol H_2O/mol dimer	7.6	12.4
$\Delta V^*_{\text{growth}}$, ml/mol dimer	**−29.8 ± 3.3**	−36.6
$\Delta a^*_{\text{growth}}$, nm^2/molecule	2.4	**2.9 ± 0.5**
$\Delta n_w^*{}_{\text{growth}}$, mol H_2O/mol dimer	18.3	22.5

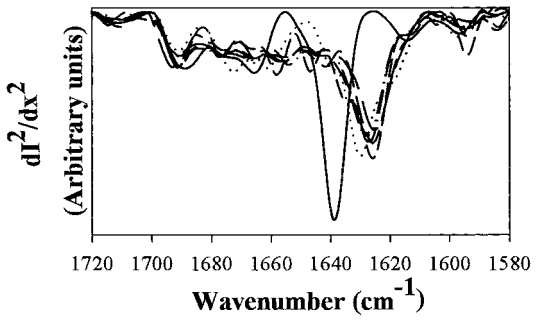

FIG. 3. **Second-derivative amide I FT-IR spectra for native SMA (*solid line*), pure SMA amyloid fibrils (*dotted line*), and pressure-induced aggregates generated at 80 (*long dashed line*), 120 (*medium dashed line*), 160 (*short dashed line*), 200 (*dashed-dotted line*), and 240 (*dashed-dotted-dotted line*) MPa.**

TABLE III
Energetic parameters for the formation of N for prenucleation assembly, nucleation, and growth of SMA aggregation*

Values were calculated at 32 °C in kJ/mol, and ± values refer to 95% confidence limits.

	E_a	ΔG^*	ΔH^*	$T\Delta S^*$	ΔG^*_{solv}	$\Delta G^*_{\text{conf}}{}^a$	$\Delta H^*_{\text{solv}}{}^a$	$\Delta H^*_{\text{conf}}{}^a$	$T\Delta S^*_{\text{solv}}$	$T\Delta S^*_{\text{conf}}{}^a$
Prenucleation assembly	119 ± 31	105 ± 31	116 ± 25	11 ± 4	68 ± 13	36 ± 34	55 ± 13	61 ± 34	−13 ± 3	24 ± 5
Nucleation	159 ± 18	96 ± 22	161 ± 18	60 ± 13	64 ± 13	32 ± 25	51 ± 14	105 ± 29	−13 ± 5	73 ± 14
Growth	156 ± 12	93 ± 13	153 ± 12	61 ± 5	124 ± 21	−31 ± 25	97 ± 22	57 ± 26	−26 ± 5	87 ± 7

[a] Values were calculated as follows: $\Delta G^*_{\text{conf}} = \Delta G^* - \Delta G^*_{\text{solv}}$; $T\Delta S^*_{\text{conf}} = T\Delta S^* - T\Delta S^*_{\text{solv}}$; $H^*_{\text{solv}} = \Delta G^*_{\text{solv}} + T\Delta S^*_{\text{solv}}$; and $\Delta H^*_{\text{conf}} = \Delta G^*_{\text{conf}} + T\Delta S^*_{\text{conf}}$.

TABLE IV

ThT fluorescence intensity for the aggregates from pressure-, temperature-, protein concentration-, and sucrose concentration-dependent aggregation of SMA

The values are means ± S.D. in arbitrary units for triple measurements. For the pure amyloid fibrils generated from 1 mg/ml SMA with agitation at 37 °C for 96 h, ThT fluorescence intensity was 21.3 ± 1.4 (13).

P[a]	ThT	T[b]	ThT	SMA[c]	ThT	Sucrose[d]	ThT
MPa		°C		*mg/ml*		M	
80	2.4 ± 1.2	30	2.5 ± 0.1	0.25	0.8 ± 0.1	0.125	2.8 ± 0.3
120	2.3 ± 0.2	32	2.8 ± 0.1	0.5	2.0 ± 0.2	0.25	2.7 ± 0.1
160	2.7 ± 0.2	34	3.0 ± 0.2	0.75	2.4 ± 0.1	0.5	2.6 ± 0.1
200	3.5 ± 0.8	36	3.0 ± 0.2	1	3.1 ± 0.1	0.75	2.1 ± 0.0
240	4.5 ± 0.1	38	3.4 ± 0.3	1.25	3.5 ± 0.1	1	1.7 ± 0.1

[a] 1 mg/ml SMA at 32 °C and 200 MPa.
[b] 1 mg/ml SMA at 200 MPa.
[c] 200 MPa and 32 °C.
[d] 1 mg/ml SMA at 200 MPa and 32 °C.

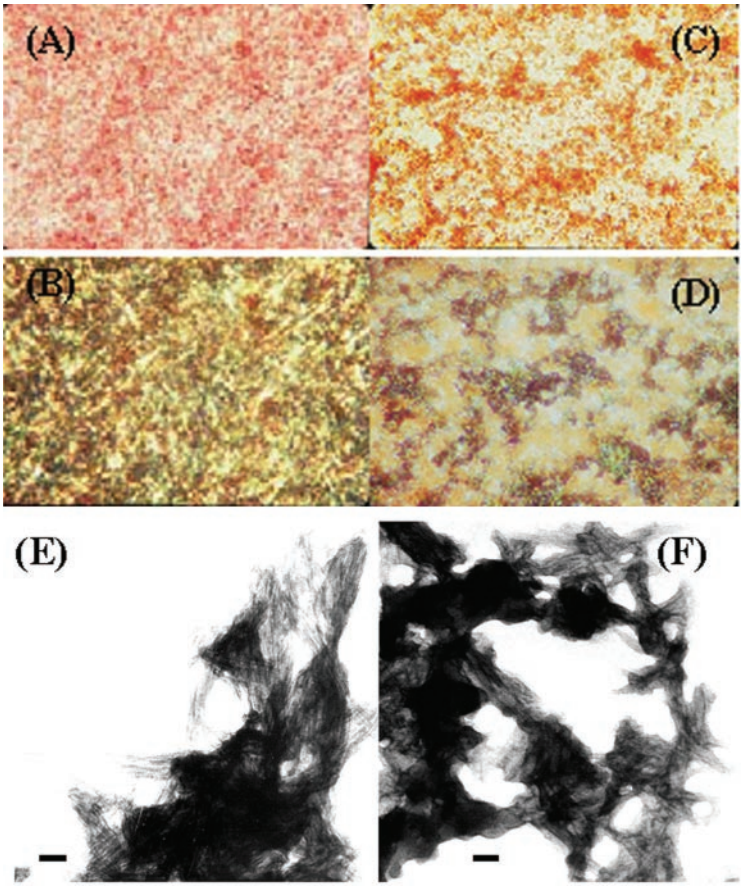

FIG. 4. **Representative images of CR staining and TEM for SMA amyloid fibrils formed at atmospheric pressure and pressure-induced aggregates (1 mg/ml SMA at 200 MPa and 32 °C).** For CR staining, images for SMA amyloid fibrils (*A* and *B*) and pressure-induced aggregates (*C* and *D*) are shown in bright-field (*A* and *C*) and under polarized light (*B* and *D*) (magnification ×200). TEM images are shown for SMA amyloid fibrils (*E*) and pressure-induced aggregates (*F*). *Scale bars* = 100 nm.

ated from the same protein concentration at atmospheric pressure by agitation for 96 h (13). CR stained the pressure-induced aggregates, but was less birefringent under polarized light compared with pure SMA amyloid fibrils (Fig. 4). TEM of a representative sample of pure SMA fibrils showed bundles containing fibrils that were unbranched and ~6–12 nm in diameter (Fig. 4*E*), which is typical of amyloid fibril morphology (27). Pressure-induced aggregates showed amorphous aggregates interspersed with bundles of amyloid fibrils that were similar in appearance to those in the pure fibril sample (Fig. 4*F*). Taken together, these results show that pressure-induced aggregates were a mixture of amyloid fibrils and amorphous aggregates. Mixed aggregate morphologies have been previously reported for LC deposits found *in vivo* (28, 29).

Effects of Seeding—Lag phases for nucleation-dependent fibril assembly can be shortened by the addition of seeds (4). Under pressure, samples seeded with pure fibrils formed at atmospheric pressure or aggregates formed at high pressure showed much shorter t_{lag} rates, but much slower growth rates compared with samples prepared without seeds (Fig. 2*C*). Interestingly, both t_{lag} and growth rates were similar after the addition of either type of seed. Both seeded aggregates were a mixture of amorphous aggregates and fibrils (data not shown). Furthermore, high pressure-induced aggregates seeded formation of amyloid fibrils at atmospheric pressure that were indistinguishable by ThT fluorescence, CR staining, and TEM from those formed without seeds (data not shown).

In Situ CR Binding Kinetics—To follow directly the formation of SMA amyloid fibrils under pressure, we incubated SMA in the presence of CR, which binds specifically to amyloid fibrils, inducing a characteristic shift in maximum absorbance from ~490 nm to ~542 nm (18). We observed such a shift as a function of time under pressure (Fig. 5*A*). To monitor the CR-specific spectral changes without interference from light scattering, we followed the time-dependent intensity of second-derivative absorbance spectra at 542 nm (Fig. 5*B*). The CR binding rate increased

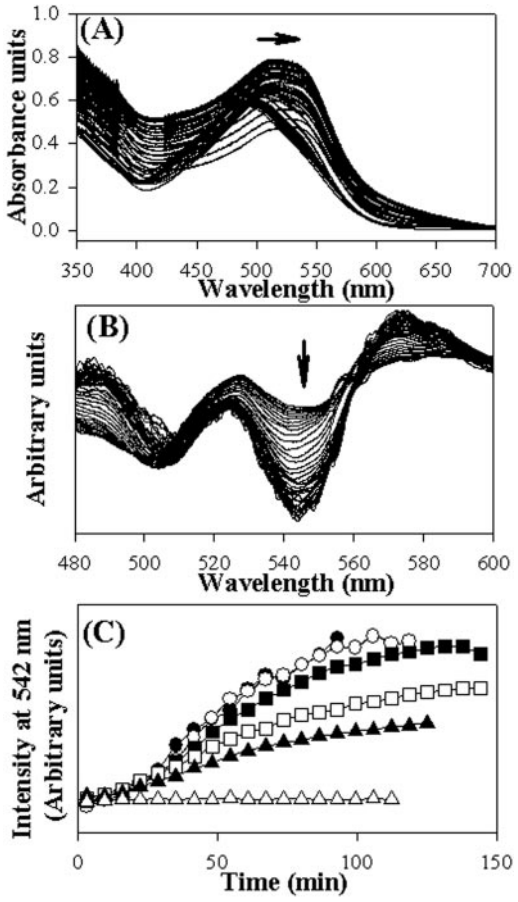

FIG. 5. ***In situ* CR binding to SMA.** *A* and *B*, representative CR absorbance spectra and second-derivative absorbance spectra, respectively, collected every 3.2 min for 120 min (1 mg/ml SMA in buffer A with 10 mM DTT at 200 MPa and 32 °C). *Arrows* indicate the direction of the spectral shift with increasing time. *C*, amyloid fibril formation kinetics monitored by the intensity at 542 nm of second-derivative absorbance spectra at pressures of 80 (▲), 120 (□), 160 (■), 200 (○), and 240 (●) MPa. Also shown are results for a non-aggregating control sample (1 mg/ml SMA in buffer A without DTT) at 200 MPa (△).

directly with pressure (Fig. 5*C*). Interestingly, lag times were greatly reduced in the presence of CR, and there was not a detectable pressure sensitivity of nucleation ($\Delta V^*_{nuc} \approx 0$). In the presence of CR, ΔV^*_{growth} was much smaller compared with that measured in the absence of CR (-12.4 ± 2.8 *versus* -29.8 ± 3.3 ml/mol, respectively). In the non-aggregating control sample, no CR absorbance shifts were noted under pressure (Fig. 5*C*). At atmospheric pressure, the addition of CR also greatly accelerated SMA amyloid fibril formation by reducing t_{lag} (data not shown).

DISCUSSION

Pressure-induced Unfolding—High pressure favors reactions that reduce the overall system volume. Two such reactions of particular importance to protein conformational changes are solvation of hydrophobic surfaces and charged residues (8, 9, 30). In contrast, formation of a hydrogen bond causes negligible system volume change and is thus largely unaffected by pressure (8, 9). ΔV_d for SMA was in the range typically found for other dimer-monomer dissociations (-50 to -200 ml/mol), but $P_{½}$ was significantly higher compared with other dimer-monomer systems (<300 MPa) (7, 10, 11). Based on the structure of the homologous V_L LEN, SMA dimers are stabilized by intersubunit hydrogen bonds, mainly contributed by Gln-38 across the interfaces (17). Thus, the abnormally high $P_{½}$ results from pressure-independent hydrogen bonds, counteracting pressure effects on electrostatic and hydrophobic interactions. Both urea and pressure unfolding experiments were consistent with a two-state model, suggesting that dissociation and unfolding occur concomitantly. Thus, the reduction in system volume under pressure can be attributed to exposure of hydrophobic surfaces and charged residues to solvent as dimers dissociate and unfold.

Aggregation and Amyloid Fibril Formation—Results at atmospheric and elevated pressures were consistent with a nucleation-dependent protein assembly mechanism in which there is a distinct lag phase, followed by nucleation and rapid growth and which can be seeded (3, 4). In the pressure studies, prenucleation assembly, nucleation, and growth showed first-order dependence on SMA concentration, suggesting that a process involving conformational change in SMA is rate-limiting for the reactions. For all three reactions, ΔV^* is negative and Δa^* is positive, documenting that N^* for each transition has more solvent-exposed residues than N. Furthermore, the magnitudes of expansion required to effect these changes are small fractions (~10–30%) of that for dissociation and unfolding, suggesting that the transition states are dimers with structure only slightly different from that of the native state. Our values of ΔV^* and Δa^* are consistent with the proposed structural model for V_L fibrillogenesis in which a small, mobile loop (22 of 216 residues) in each dimer becomes solvent-exposed, allowing domain swapping (31). Previously, we showed that formation of the transition state for interferon-γ aggregation also requires a minor conformational change in the dimer (11). A dimeric transition state may subsequently dissociate into a monomeric aggregation-competent species, which has been suggested to be the precursor for fibril formation by proteins such as LCs (13, 15) and transthyretin (32).

The values of ΔV^* and Δa^* are comparable for prenucleation assembly and nucleation, but are about half those for growth (Table II). Formation of the transition state for fibril growth thus requires a larger conformational change, the exact nature of which is not known, although it is still small compared with dissociation and unfolding. ΔG^* values for prenucleation assembly, nucleation, and growth were similar (Table III), even though N^* for growth appears to be more structurally perturbed than N^* for prenucleation assembly and nucleation. Greater structural perturbation of N^* for growth is reflected in the negative value of, and a dominant entropic contribution to, ΔG^*_{conf} for the growth phase. ΔG^*_{conf} values for prenucleation assembly and nucleation are small, with similar, opposing entropic and enthalpic contributions. Hydration of the transition state is more limiting for growth than for the other processes, as shown by its relatively large value of ΔG^*_{solv}. For all transitions, formation of N^* is limited by the relatively large ΔH^*. This enthalpic penalty for formation of the transition states is augmented by the loss of entropy associated with solvation of N^* and partially offset by an increase in $T\Delta S^*_{conf}$, as the protein conformation is disordered.

CR Binding Studies—In situ CR binding showed that CR is not an inert reporter of fibril formation. Rather, the addition of CR decreased the energy barrier for nucleation (as evidenced by shortened lag phases) and also greatly reduced pressure sensitivity of nucleation ($\Delta V^*_{nuc} \approx 0$). CR binds to LC dimers to populate molten globule-like intermediates (33). CR also binds to SMA (34). The CR·SMA complex presumably has a perturbed structure, minimizing the additional conformational changes required to form N^* for nucleation. Similarly, ΔV^*_{growth} in the presence of CR is about half that in the absence of CR, suggesting that the CR·SMA complex must undergo a smaller conformational change to reach N^* than that for SMA alone. The effects of CR on both protein structure and assembly call into questions the proposed therapeutic uses of this compound

or its analogs as inhibitors of amyloid fibril formation (35, 36).

Conclusion—Relatively minor conformational perturbations may provide the rate-limiting step for protein nucleation (3, 4), aggregation (11, 12), and fibril formation (1, 2, 6, 32). Our results show that the transition states for prenucleation assembly, nucleation, and growth of SMA aggregates have conformations that are similar to the native state. Therefore, genetic or environmental (*e.g.* urea in the kidney (13) or exogenous CR) factors that even minimally perturb the native state may significantly populate such transition state species, resulting in rapid fibril formation.

Acknowledgments—We thank Willy Grothe and Matthew Seefeldt for fabrication of the high-pressure UV cell, Dr. Judith Snyder (University of Denver) for polarization microscopy, and Dot Dill and Dr. Steve Cape for help with TEM. Drs. Aichun Dong and Jonathan Wall provided helpful discussions on FT-IR data and TEM images, respectively.

REFERENCES

1. Wetzel, R. (1996) *Cell* **86,** 699–702
2. Wetzel, R. (1997) *Adv. Protein Chem.* **50,** 183–242
3. Jarrett, J. T., Berger, E. P., and Lansbury, P. T., Jr. (1993) *Biochemistry* **32**, 4693–4697
4. Harper, J. D., and Lansbury, P. T., Jr. (1997) *Annu. Rev. Biochem.* **66**, 385–407
5. Speed, M. A., Wang, D. I., and King, J. (1996) *Nat. Biotechnol.* **14,** 1283–1287
6. Fink, A. (1998) *Fold. Des.* **3,** R9–R23
7. Silva, J. L., and Weber, G. (1993) *Annu. Rev. Phys. Chem.* **44,** 89–113
8. Gross, M., and Jaenicke, R. (1994) *Eur. J. Biochem.* **221,** 617–630
9. Mozhaev, V. V., Heremans, K., Frank, J., Masson, P., and Balny, C. (1996) *Proteins Struct. Funct. Genet.* **24,** 81–91
10. Silva, J. L., Foguel, D., and Royer, C. A. (2001) *Trends Biochem. Sci.* **26,** 612–618
11. Webb, J. N., Webb, S. D., Cleland, J. L., Carpenter, J. F., and Randolph, T. W. (2001) *Proc. Natl. Acad. Sci. U. S. A.* **98,** 7259–7264
12. Kendrick, B., Carpenter, J. F., Cleland, J. L., and Randolph, T. W. (1998) *Proc. Natl. Acad. Sci. U. S. A.* **95,** 14142–14146
13. Kim, Y.-S., Cape, S. P., Chi, E., Raffen, R., Wilkins-Stevens, P., Stevens, F. J., Manning, M. C., Randolph, T. W., Solomon, A., and Carpenter, J. F. (2001) *J. Biol. Chem.* **276,** 1626–1633
14. Wilkins-Stevens, P., Raffen, R., Hanson, D. K., Deng, Y. L., Berrios-Hammond, M., Westholm, F. A., Murphy, C., Eulitz, M., Wetzel, R., Solomon, A., Schiffer, M., and Stevens, F. J. (1995) *Protein Sci.* **4,** 421–432
15. Khurana, R., Gillespie, J. R., Talapatra, A., Minert, L. J., Ionescu-Zanetti, C., Millett, I., and Fink, A. L. (2001) *Biochemistry* **40,** 3525–3535
16. Ragone, R., Colonna, G., Balestrieri, C., Servillo, L., and Irace, G. (1984) *Biochemistry* **23,** 1871–1875
17. Huang, D. B., Chang, C. H., Ainsworth, C., Johnson, G., Solomon, A., Stevens, F. J., and Schiffer, M. (1997) *Mol. Immunol.* **34,** 1291–1301
18. Klunk, W. E., Jacob, R. F., and Mason, R. P. (1999) *Methods Enzymol.* **309,** 285–305
19. Kim, Y.-S., Wall, J. S., Meyer, J., Murphy, C., Randolph, T. W., Manning, M. C., Solomon, A., and Carpenter, J. F. (2000) *J. Biol. Chem.* **275,** 1570–1574
20. Solomon, A., Weiss, D. T., Murphy, C. L., Hrncic, R., Wall, J. S., and Schell, M. (1998) *Proc. Natl. Acad. Sci. U. S. A.* **95,** 9547–9551
21. Pace, C. N. (1986) *Methods Enzymol.* **131,** 266–280
22. Supran, M. K., Acton, J. C., Howell, A. J., and Saffle, R. L. (1971) *J. Milk. Food Technol.* **34,** 584–585
23. Smith, J. M. (1956) in *Chemical Engineering Series* (Kirkpatrick, S. D., ed) pp. 41–84, McGraw-Hill Inc., New York
24. Vargaftik, N. B., Volkov, B. N., and Voljak, L. D. (1983) *J. Phys. Chem. Ref. Data* **12,** 817–820
25. Ashbaugh, H. S., and Paulaitis, M. E. (1996) *J. Phys. Chem.* **100,** 1900–1913
26. Dong, A., Prestrelski, S. J., Allison, S. D., and Carpenter, J. F. (1995) *J. Pharm. Sci.* **84,** 415–424
27. Sunde, M., and Blake, C. F. (1998) *Q. Rev. Biophys.* **31,** 1–39
28. Kaplan, B., Vidal, R., Kumar, A., Ghiso, J., Frangione, B., and Gallo, G. (1997) *Clin. Exp. Immunol.* **110,** 472–478
29. Stokes, M. B., Jagirdar, J., Burchstin, O., Kornnacki, S., Kumar, A., and Gallo, G. (1997) *Mod. Pathol.* **10,** 1059–1065
30. Hummer, G., Garde, S., Garcia, A. E., Paulaitis, M. E., and Pratt, L. R. (1998) *Proc. Natl. Acad. Sci. U. S. A.* **95,** 1552–1555
31. Davis, P. D., Raffen R., Dul, L. J., Vogen, M. S., Williamson, K. E., Stevens, F. J., and Argon, Y. (2000) *Immunity* **13,** 433–442
32. Kelly, J. W. (1998) *Curr. Opin. Struct. Biol.* **8,** 101–106
33. Piekarska, B., Skowronek, M., Rybarska, J., Stopa, B., Roterman, I., and Konieczny, L. (1996) *Biochimie* (*Paris*) **78,** 183–189
34. Khurana, R., Uversky, V. N., Nielsen, L., and Fink, A. L. (2001) *J. Biol. Chem.* **276,** 22715–22721
35. Findeis, M. A. (2000) *Biochim. Biophys. Acta* **1502,** 76–84
36. Rudyk, H., Vasiljevic, S., Hennion, R. M., Birkett, C. R., Hope, J., and Gilbert, I. H. (2000) *J. Gen. Virol.* **81,** 1155–1164